Myeloid-derived suppressor cells inhibit T cell activation through nitrating LCK in mouse cancers

Shan Feng[a,b,c,d,1,2], Xi Cheng[a,b,c,e,1], Lin Zhang[d], Xuemin Lu[a,b,c], Seema Chaudhary[a,b,c], Ruifang Teng[d], Christian Frederickson[a,b,c], Matthew M. Champion[b,f], Ren Zhao[e], Liang Cheng[g], Yiyi Gong[h], Haiteng Deng[d], and Xin Lu[a,b,c,i,3]

[a]Department of Biological Sciences, University of Notre Dame, Notre Dame, IN 46556; [b]Boler–Parseghian Center for Rare and Neglected Diseases, University of Notre Dame, Notre Dame, IN 46556; [c]Harper Cancer Research Institute, University of Notre Dame, Notre Dame, IN 46556; [d]Ministry of Education Key Laboratory of Bioinformatics, School of Life Sciences and Tsinghua University–Peking University Joint Center for Life Sciences, Tsinghua University, 100084 Beijing, China; [e]Department of General Surgery, Ruijin Hospital, Shanghai Jiao Tong University School of Medicine, 200025 Shanghai, China; [f]Department of Chemistry and Biochemistry, University of Notre Dame, Notre Dame, IN 46556; [g]Department of Pathology and Laboratory Medicine, Indiana University School of Medicine, Indianapolis, IN 46202; [h]Central Research Laboratory, Peking Union Medical College Hospital, Chinese Academy of Medical Sciences and Peking Union Medical College, 100730 Beijing, China; and [i]Tumor Microenvironment and Metastasis Program, Indiana University Melvin and Bren Simon Cancer Center, Indianapolis, IN 46202

Edited by Ronald A. DePinho, The University of Texas MD Anderson Cancer Center, Houston, TX, and approved August 21, 2018 (received for review January 12, 2018)

Potent immunosuppressive mechanisms within the tumor microenvironment contribute to the resistance of aggressive human cancers to immune checkpoint blockade (ICB) therapy. One of the main mechanisms for myeloid-derived suppressor cells (MDSCs) to induce T cell tolerance is through secretion of reactive nitrogen species (RNS), which nitrates tyrosine residues in proteins involved in T cell function. However, so far very few nitrated proteins have been identified. Here, using a transgenic mouse model of prostate cancer and a syngeneic cell line model of lung cancer, we applied a nitroproteomic approach based on chemical derivation of 3-nitrotyrosine and identified that lymphocyte-specific protein tyrosine kinase (LCK), an initiating tyrosine kinase in the T cell receptor signaling cascade, is nitrated at Tyr394 by MDSCs. LCK nitration inhibits T cell activation, leading to reduced interleukin 2 (IL2) production and proliferation. In human T cells with defective endogenous LCK, wild type, but not nitrated LCK, rescues IL2 production. In the mouse model of castration-resistant prostate cancer (CRPC) by prostate-specific deletion of *Pten*, *p53*, and *Smad4*, CRPC is resistant to an ICB therapy composed of antiprogrammed cell death 1 (PD1) and anticytotoxic–T lymphocyte-associated protein 4 (CTLA4) antibodies. However, we showed that ICB elicits strong anti-CRPC efficacy when combined with an RNS neutralizing agent. Together, these data identify a previously unknown mechanism of T cell inactivation by MDSC-induced protein nitration and illuminate a clinical path hypothesis for combining ICB with RNS-reducing agents in the treatment of CRPC.

myeloid-derived suppressor cells | protein nitration | LCK | prostate cancer | immune checkpoint blockade

Inhibition of cytotoxic T lymphocytes by immunosuppressive cells represents a significant contributing mechanism to immunotherapy resistance (1). Among the immunosuppressive cells, myeloid-derived suppressor cells (MDSCs) are immature myeloid cells that maintain T cell tolerance (2, 3). Activation of MDSCs is usually manifested by up-regulation of arginase 1 (ARG1) and inducible nitric oxide synthase (iNOS), as well as increased production of reactive oxygen species (ROS) and reactive nitrogen species (RNS) such as peroxynitrite (2). MDSCs are phenotypically divided into granulocytic (Gr-MDSCs) and monocytic (Mo-MDSCs) subpopulations (2). Both MDSC subgroups inhibit T cells through NO-related pathways, and the primary mechanism by Gr-MDSCs is through production of ROS and RNS (4). RNS has emerged as a potent chemical modifier to induce nitration of chemokines and receptors on T cells, creating a "chemical barrier" to restrict T cell infiltration and impair T cell functions (5).

Protein nitration, a form of posttranslational modification, usually occurs at the 3′-position of the phenolic ring of tyrosine (Tyr) to form 3-nitrotyrosine (3-NT). Up-regulation of 3-NT is documented in various human cancers, including prostate cancer (6–9). In MDSCs, both endothelial NO synthase (eNOS) and iNOS contribute to the production of NO. NO reacts with superoxide $O_2^{\bullet-}$ rapidly and forms RNS such as peroxynitrite ($ONOO^-$) and the free radical nitrogen dioxide ($\bullet NO_2$), which lead to Tyr nitration (5, 10, 11). Due to the different chemical properties between Tyr and 3-NT, a nitrated protein may have perturbed signaling activity (10, 11). Tyr nitration has been documented to either positively or negatively regulate Tyr phosphorylation (12, 13). Protein nitration as a type of oxidative damage is highly relevant to aging and diseases including cancer (10, 11). MDSC-derived peroxynitrite could cause nitration of the T cell receptor (TCR)–CD8 complex and reduce its binding to peptide–major histocompatibility complex (14). Nitration of CCL2 by MDSC-derived peroxynitrite impairs the infiltration of effector $CD8^+$ T cells (7). Previous studies also showed that peroxynitrite

Significance

Immune checkpoint blockade (ICB) to reinvigorate cytotoxic T lymphocytes using antibodies against CTLA4 or PD1 generates durable therapeutic responses in patients across a variety of cancer types. However, some cancers such as castration-resistant prostate cancer (CRPC) show overwhelming resistance to ICB. Here, we develop a nitroproteomic approach and uncover a potential mechanism for the immunotherapy resistance where a key protein for T cell activation, lymphocyte-specific protein tyrosine kinase (LCK), is nitrated and inactivated by myeloid-derived suppressor cell–generated reactive nitrogen species (RNS) in the resistant tumor. An agent that neutralizes RNS significantly sensitizes CRPC to ICB therapy in a mouse model. Therefore, our studies illuminate a clinical path hypothesis for combining ICB with RNS-reducing agents in the treatment of ICB-resistant cancers.

Author contributions: S.F. and Xin Lu designed research; S.F., X.C., L.Z., Xuemin Lu, S.C., R.T., C.F., M.M.C., Y.G., and Xin Lu performed research; L.C. contributed reagents; S.F. and Xin Lu analyzed data; S.F. and Xin Lu wrote the paper; and R.Z., H.D., and Xin Lu supervised the research.

The authors declare no conflict of interest.

This article is a PNAS Direct Submission.

Published under the PNAS license.

[1]S.F. and X.C. contributed equally to this work.

[2]Present address: Mass Spectrometry Core Facility, Institute for Biology, Westlake Institute for Advanced Study, Hangzhou, 310024 Zhejiang, China.

[3]To whom correspondence should be addressed. Email: xlu@nd.edu.

This article contains supporting information online at www.pnas.org/lookup/suppl/doi:10.1073/pnas.1800695115/-/DCSupplemental.

Published online September 19, 2018.

perturbed Tyr phosphorylation and inhibited T cell activation (6, 15). However, these studies did not identify specific nitrated Tyr sites on proteins involved in T cell function. To identify the precise 3-NT sites, a global mass spectrometry (MS)-based profiling approach is needed. However, mapping nitration sites is challenging, due to low abundance of this modification in biological samples (16). Currently, an enrichment technique followed by MS is the most powerful approach for detecting nitropeptides. Enrichment procedures include use of either 3-NT specific antibodies or chemical derivation that reduces a nitro group to an amine group (17–19). Most previous studies aimed at methodology development and used in vitro overnitrated samples to profile artificially nitrated instead of endogenously nitrated proteins.

In this study, we developed a chemical derivation method to profile endogenous nitropeptides from tumor-infiltrating T cells of two cancer models and identified a shared nitration site at lymphocyte-specific protein tyrosine kinase (LCK) (Tyr394) with functional impact. We showed the accumulation of 3-NT in clinical samples of castration-resistant prostate cancer (CRPC), a lethal disease overwhelmingly resistant to immune checkpoint blockade (ICB) (20). Importantly, in a CRPC mouse model we recently developed (21), CRPC can be sensitized to ICB treatment when RNS is neutralized in a combination therapy setting.

Results

Induction of Protein Nitration by Intratumoral MDSCs. We first compared the concentration of nitrite between spontaneous prostate tumors from the Pten/p53/Smad4 model (21, 22) and normal prostate from age-matched wild-type C57BL/6 mice, as well as between Lewis lung carcinoma (LLC) s.c. tumors and normal lung from age-matched C57BL/6 mice. In both cases, the tumor lysates contained four- to sixfold higher nitrite level compared with normal tissues (Fig. 1*A*). In accordance with increased nitrite level, Pten/p53/Smad4 and LLC tumors exhibited significantly augmented 3-NT level detected by immunoblot (Fig. 1 *B* and *C*) and immunohistochemistry (*SI Appendix*, Fig. S1*A*). The 3-NT signals were attenuated by $Na_2S_2O_4$ treatment, which reduces 3-NT to 3-aminotyrosine. To examine the relative contribution of tumor and stromal compartments to the 3-NT signals, we utilized the Pten/p53/Smad4/mTmG model (21), which allowed separation of GFP^+ tumor cells and $tdTomato^+$ stromal cells. The result showed that both compartments contained significant level of 3-NT (*SI Appendix*, Fig. S1*B*). MDSC infiltration was reported in both Pten/p53/Smad4 model and LLC model: in the case of Pten/p53/Smad4 prostate tumors, we recently identified Gr-MDSCs as the dominant intratumoral MDSC population (21); in the case of LLC tumors, comparable frequency of Gr-MDSCs and Mo-MDSC were detected (*SI Appendix*, Fig. S1*C*), consistent with previous report (23). Compared with circulating neutrophils from tumor-free mice, both Gr-MDSCs and Mo-MDSCs from the LLC model generated dramatically increased amount of nitrite, with Mo-MDSCs producing moderately higher (*SI Appendix*, Fig. S1*D*), a result consistent with previous report (4). We also isolated intratumoral MDSCs and tumor-associated macrophages (TAMs) from $CD11b^+$ cell populations in both models and found that MDSCs produced a higher level of nitrite compared with TAMs (*SI Appendix*, Fig. S1 *E* and *F*).

To show whether MDSCs induce protein nitration in T cells, we isolated total T cells from spleen of wild-type mice, activated with anti-CD3/anti-CD28 antibodies in the presence or absence of coculture with MDSCs isolated from the spleen or primary prostate tumors of the Pten/p53/Smad4 model. The T cells were subsequently isolated from the coculture for Western blot of 3-NT. Peroxynitrite treatment in the process of T cell activation was used as a positive control. The 3-NT bands were detected by both splenic and intratumoral MDSC coculture, although intratumoral MDSCs induced stronger 3-NT signals (Fig. 1*D*). The protein nitration returned to basal level when uric acid (UA), a potent peroxynitrite neutralizer (14), was added to the coculture of T cells with intratumoral MDSCs. Induced T cell activation turned on production of IL2, which was largely abrogated by intratumoral

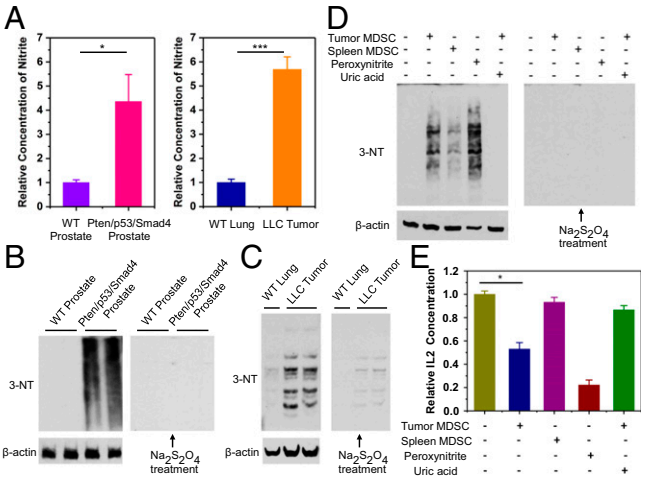

Fig. 1. Intratumoral MDSCs induce protein nitration. (*A*) Comparison of relative nitrite concentration in Pten/p53/Smad4 spontaneous tumor with wild-type (WT) prostate (*Left*) and LLC s.c. tumor with WT lung (*Right*) (n = 3). (*B*) Western blot of 3-NT of WT prostate and Pten/p53/Smad4 spontaneous tumor. (*C*) Western blot of 3-NT of WT lung and LLC s.c. tumor. $Na_2S_2O_4$ treatment of the blot membrane converted 3-NT to 3-aminotyrosine and eliminated signals. (*D*) Primary T cells isolated from WT mouse spleen were stimulated by anti-CD3/CD28 condition for 48 h in the absence or presence of MDSCs isolated from Pten/p53/Smad4 tumor or spleen. Peroxynitrite at 50 μM or uric acid at 50 μM were added as indicated. Whole cell lysates of isolated T cells were immunoblotted for 3-NT. (*E*) Primary T cells were treated as in *D*, and the IL2 concentration of each sample was measured in the medium using ELISA (n = 2). In *A* and *E*, data represent mean ± SD. $^*P < 0.05$, $^{***}P < 0.001$, Student's t test.

MDSC coculture or peroxynitrite treatment (Fig. 1*E*). Activation markers for cytotoxic T cells, including INF-γ, perforin, and granzyme B, were also down-regulated by MDSC coculture or peroxynitrite treatment (*SI Appendix*, Fig. S1*G*). Intratumoral MDSCs isolated from LLC tumors also induced 3-NT signals and reduced IL2 production in T cells (*SI Appendix*, Fig. S1 *H* and *I*). Together, these data showed induction of protein nitration and correspondingly reduced IL2 secretion in T cells by intratumoral MDSCs in two independent mouse models.

Development of a Method for Nitropeptide Profiling. To identify specific nitration sites, we developed a method of nitropeptide enrichment and profiling. We used Angiotensin II (Ang II) as the model peptide for the methodology development (Fig. 2*A*). Ang II was nitrated by peroxynitrite, followed by alkylation using formaldehyde to block the primary amine. Next, 3-NT was reduced by $Na_2S_2O_4$ to generate 3-aminotyrosine, which was further labeled with NHS-S-S-biotin and enriched by streptavidin beads. For the detection, the enriched peptides were eluted by dithiothreitol (DTT) and modified by iodoacetamide (IAA). The final product was analyzed by liquid chromatography–tandem mass spectrometry (LC-MS/MS). The monoisotope peak of Ang II was at 523.78 m/z with duple charge (*SI Appendix*, Fig. S2 *A*, *i*), and the fragmentation pattern of this peptide was featured by the two highest peaks in the low m/z range: y_2 ion at 263.14 and immonium ion of His at 110.07 (*SI Appendix*, Fig. S2*B*). After nitration by peroxynitrite, the monoisotope peak with the duple charge shifted to 546.28 m/z, indicating 45 Da larger than the original Ang II (*SI Appendix*, Fig. S2 *A*, *ii*). Dimethyl labeling and reduction of the nitro group increased the molecule weight by 28 Da (560.29 m/z) and reduced it by 30 Da (545.31 m/z), respectively (*SI Appendix*, Fig. S2 *A*, *iii* and *iv*). All of the MS/MS of these intermediate products were shown in *SI Appendix*, Fig. S2 *C–E*. After the peptide enrichment, reduction, and alkylation, the monoisotope peak of the final product was detected at 617.82 m/z with duple charge, which corresponded to a +160 Da

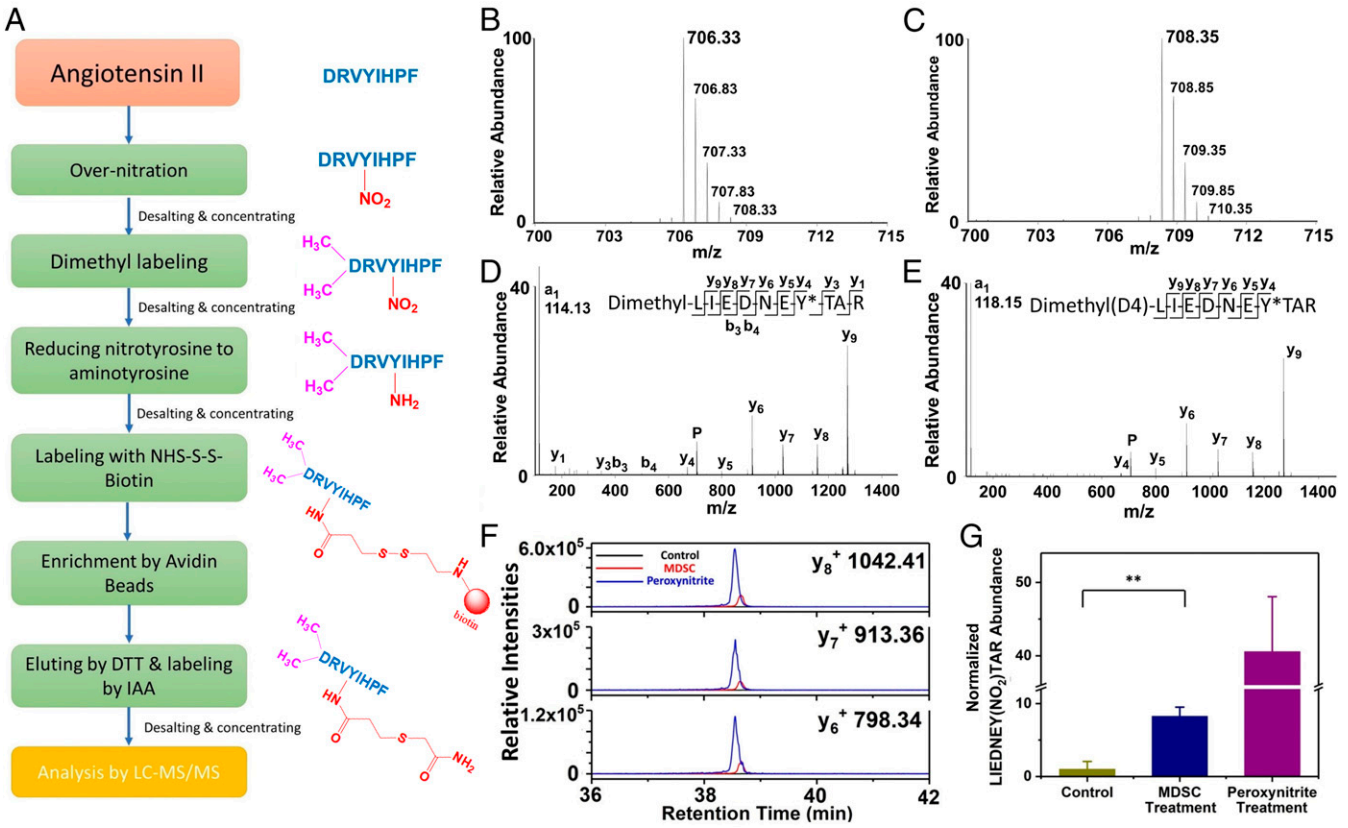

Fig. 2. Methods for nitropeptide enrichment and identification of nitro-Tyr394 peptide LIEDNEYTAR in LCK from both mouse models. (*A*) The workflow of the chemical derivation method for detecting nitrated Ang II. (*B*) The MS of the modified LCK peptide from T cells of the Pten/p53/Smad4 tumors. The monoisotope peak at *m/z* 706.33 matched the duple-charged, CH_2O-labeled peptide. (*C*) The MS of the modified LCK peptide from T cells of the LLC tumors. The monoisotope peak at *m/z* 708.35 matched to the duple-charged, CD_2O-labeled peptide. (*D* and *E*) The MS/MS of *B* and *C*, respectively. (*F*) The intensities of y_6, y_7, and y_8 ions of LIEDNEY(nitro)TAR in stimulated T cells (black), stimulated T cells cocultured with MDSCs (red) and stimulated T cells treated with peroxynitrite (blue) ($n = 3$). The data were acquired by MRM-MS, and each sample was performed by two technical replicates. (*G*) Normalized abundance of LIEDNEY(nitro)TAR in three cell conditions as in *F* by using two reference peptides from actin (see *Methods*). Data represent mean ± SD. $^{**}P < 0.01$, Student's *t* test.

modification on Tyr residue (*SI Appendix*, Fig. S2 *A*, *v*). The fragmentation spectrum of the final product also confirmatively showed the characteristic peaks of Ang II (y_2 ion, immonium ion of His) and was composed of the mixed pattern of a, b series ions and c_0, α cleavage at the N terminus of the peptide (*SI Appendix*, Fig. S2*F*). Together, this chemical modification method allowed us to enrich nitropeptides for the unbiased profiling purpose.

Identification of Protein Nitration at LCK (Tyr394). We applied the aforementioned methodology and focused on profiling nitropeptides of tumor-infiltrating T lymphocytes isolated from both Pten/p53/Smad4 and LLC models, with total resting splenic T cells from tumor-free C57BL/6 mice as control. For the Pten/p53/Smad4 model, intratumoral T cell lysate and normal T cell lysate were labeled with light and heavy formaldehyde, respectively. Conversely, for the LLC model, intratumoral T cell lysate and normal T cell lysate were labeled with heavy and light formaldehyde, respectively. The enriched peptides were injected into Q Exactive MS instrument, and pFind Studio software was used for the proteomic data search by adding +160 Da modification on Tyr residues. We identified 14 nitropeptides from the Pten/p53/Smad4 model and 12 nitropeptides from the LLC model (*SI Appendix*, Fig. S3). The proteins containing the nitropeptides are involved in cellular mechanisms such as metabolism, signal transduction, cytoskeletal motility, and protein degradation. Surprisingly, we identified a unique overlap of these two lists, LIEDNEY*TAR, of which the Tyr residue is the 394th residue of lymphocyte-specific protein tyrosine kinase (LCK). Specifically, the monoisotope peaks at 706.33 and 708.35 *m/z* with duple charge indicated the light and heavy formaldehyde-labeled peptides in Pten/p53/Smad4 and LLC tumor samples, respectively (Fig. 2 *B* and *C*). Both MS/MS showed the fragmentation pattern that matched the y series of ions, which further validated Tyr394 of LCK as a commonly nitrated protein in T cells from both tumor models (Fig. 2 *D* and *E*). To directly test whether MDSCs induce Tyr394 nitration on LCK in T cells, we used multiple reaction monitoring (MRM)-MS and quantified the relative amount of the LCK peptide, LIEDNEY(nitro)TAR, from anti-CD3/CD28–stimulated splenic T cells under conditions of no treatment, MDSC coculture, and peroxynitrite treatment. For each of the y_6, y_7, and y_8 ions, almost no peaks were detected in untreated condition, whereas MDSC coculture or peroxynitrite treatment induced dramatic increase of the specific nitropeptide (Fig. 2 *F* and *G*). Our results indicate that RNS produced by MDSCs can induce LCK Tyr394 nitration on mouse primary T cells.

LCK Nitration Suppresses T Cell Activation. LCK is an Src-family protein kinase and serves as the initiating tyrosine kinase in the TCR activation pathway (Fig. 3*A*). Similarly to Src, LCK activity is regulated by tyrosine phosphorylation at two sites, but with opposing effects: autophosphorylation on Tyr394 up-regulates the catalytic activity, while phosphorylation on Tyr505 down-regulates the activity (24). We hypothesized that Tyr394 nitration might lead to attenuated LCK activity and dampened TCR signaling. We used the immortalized human T cell line Jurkat to study how peroxynitrite and LCK nitration affect T cell function. While moderate concentrations of peroxynitrite (5 μM, 10 μM) did not affect Jurkat cell proliferation, high peroxynitrite (≥25 μM) showed dose-dependent inhibitory effect on Jurkat cell proliferation (*SI Appendix*, Fig. S4*A*).

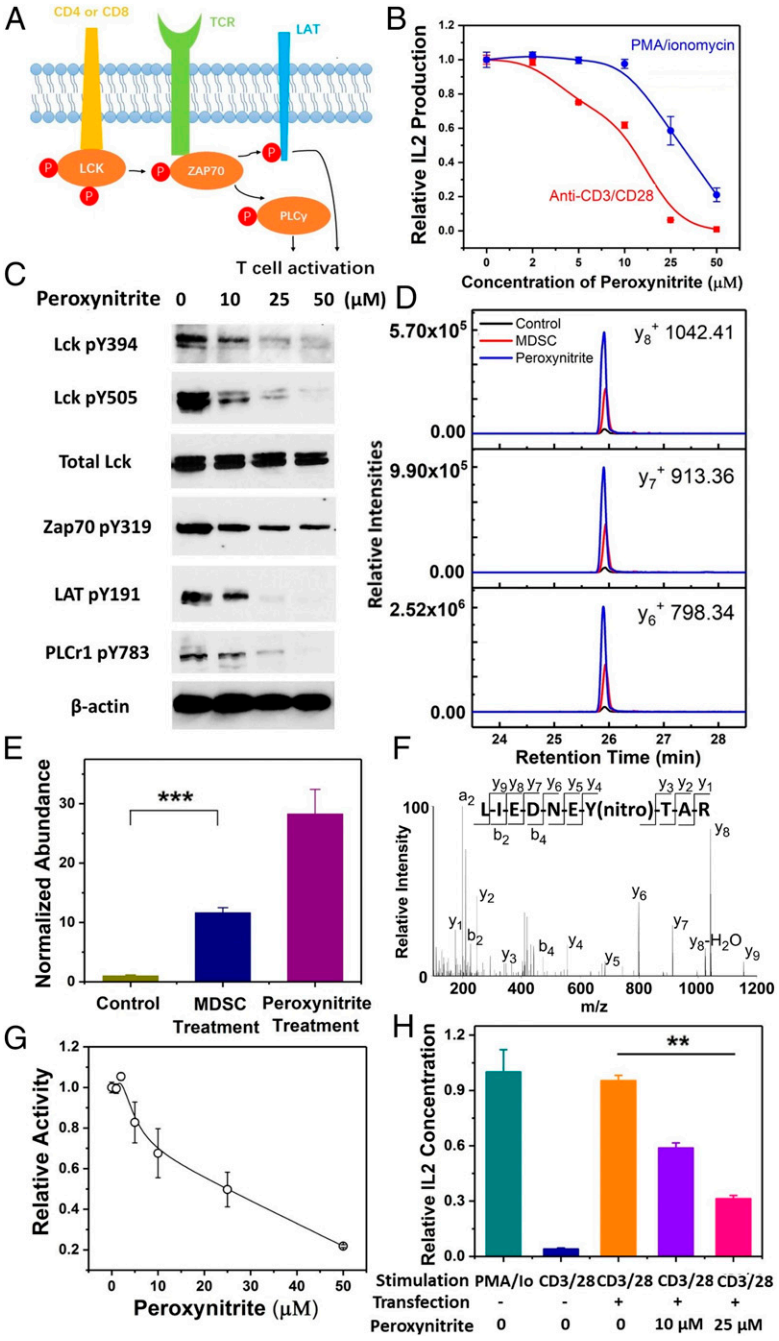

Fig. 3. Effects of nitration on LCK and T cell activation. (*A*) Brief scheme of T cell activation pathway. (*B*) Relative IL2 concentration in medium of Jurkat cells stimulated with PMA/ionomycin (blue) or anti-CD3/CD28 antibodies (red) in the presence of different concentrations of peroxynitrite, measured by ELISA ($n = 2$). (*C*) Immunoblot analysis of phosphotyrosine levels of a number of signaling proteins in the T cell activation pathway, with lysates purified from Jurkat cells stimulated with anti-CD3/CD28 antibodies in the presence of peroxynitrite. (*D*) The intensities of y_6, y_7, and y_8 ions of LIEDNEY(nitro)TAR in stimulated primary human T cells (black), stimulated T cells cocultured with MDSCs from Pten/p53/Smad4 tumors (red), and stimulated T cells treated with peroxynitrite (blue) ($n = 3$). The data were acquired by MRM-MS, and each sample had two technical replicates. (*E*) Normalized abundance of LIEDNEY(nitro)TAR in three cell conditions as in *D* by using two reference peptides from actin. (*F*) The MS/MS of tryptic nitro–Tyr394-containing peptide in recombinant LCK. The parent ion is at 634.79 *m/z* in duple charge. (*G*) Relative in intro enzymatic activity of recombinant human LCK inducted with different concentrations of peroxynitrite. Under each concentration of peroxynitrite treatment, the enzyme activity was measured twice. (*H*) Effect on IL2 production by J.CaM1.6 cells, which were stimulated with anti-CD3/CD28 antibodies and transfected with unmodified or nitrated LCK. Data were normalized to PMA/inomycin stimulation ($n = 3$). In *B*, *E*, *G*, and *H*, data represent mean ± SD. $^{**}P < 0.01$, $^{***}P < 0.001$, Student's *t* test.

Jurkat cells can be stimulated to produce IL2 by either anti-CD3/CD28 antibodies or phorbol 12-myristate 13-acetate (PMA)/ionomycin. We found that peroxynitrite modulated the IL2 production by Jurkat cells in a stimulation-specific manner: inhibition of T cell activation (indicated by lowered IL2 production) was more sensitive to peroxynitrite when Jurkat were stimulated by anti-CD3/CD28 compared with stimulation by PMA/ionomycin (Fig. 3*B*). Because anti-CD3/CD28 stimulation occurs at the most upstream of the TCR signaling pathway, whereas PMA/ionomycin bypasses the early steps and directly triggers PKC activation and Ca^{2+} release, we argue that the primary effect of peroxynitrite was due to inactivation of the upstream signaling mediators, including LCK. To test this hypothesis, we surveyed the status of a number of upstream components of the TCR signaling pathway and detected consistent down-regulation of phospho-LCK (Tyr394, Tyr505), phospho-Zap70 (Tyr319), phospho-LAT (Tyr191), and phospho-PLCγ1 (Tyr783) as a response to peroxynitrite treatment in anti-CD3/CD28–stimulated Jurkat cells (Fig. 3*C*). Concomitantly, peroxynitrite induced the formation of nitrated LCK, indirectly detected by immunoprecipitation of LCK and immunoblot of 3-NT (*SI Appendix*, Fig. S4*B*). Because there are differences in the phosphorylation cascade of the T cell activation pathway between the Jurkat cell line and primary T cells (25), human primary T cells were purified from peripheral blood mononuclear cells (PBMCs), activated with anti-CD3/CD28 antibodies, and treated by peroxynitrite. Similar to Jurkat cells, phosphorylation of LCK, Zap70, LAT, and PLCγ1 was attenuated by peroxynitrite (*SI Appendix*, Fig. S4*C*). By coculturing human primary T cells with intratumoral MDSCs from the Pten/p53/Smad4 model, we detected more than 10-fold increase of nitro-Tyr394 LCK peptide LIEDNEY(nitro)TAR using MRM (Fig. 3 *D* and *E*).

To study LCK nitration in a cell-free system, we treated recombinant human LCK protein with 50 μM peroxynitrite, and the Tyr394 nitration site was readily detected by MS (Fig. 3*F*), in addition to two other previously uncharacterized nitration sites Tyr192 and Tyr414 (*SI Appendix*, Fig. S4 *D* and *E*). To demonstrate that nitration causes "loss of function" of LCK, we generated in vitro nitrated LCK with different concentrations of peroxynitrite and measured its catalytic activity in comparison with untreated LCK protein. When peroxynitrite concentration was below 50 μM, nitration caused a dose-dependent reduction of LCK activity (Fig. 3*G*). Surprisingly, when peroxynitrite concentration was above 100 μM (i.e., at the level with significant cytotoxicity to T cells), LCK activity recovered and gradually reached an even higher level than no treatment control (*SI Appendix*, Fig. S4*F*; see *Discussion*). The inhibitory effect of nitration on LCK was further assessed in a functional rescue experiment using the J.CaM1.6 cell line. J.CaM1.6 is a derivative mutant of Jurkat with a defective LCK and inability to produce IL2 upon anti-CD3/CD28 stimulation (26). Transfection of J.CaM1.6 with untreated recombinant LCK rescued the IL2 production by anti-CD3/CD28 stimulation to the level comparable with PMA/ionomycin stimulation (Fig. 3*H*). However, LCK pretreated with 10 or 25 μM peroxynitrite partially lost the ability to rescue IL2 production (Fig. 3*H* and *SI Appendix*, Fig. S4*G*).

To investigate whether phosphorylation on Tyr394 is adversely affected by peroxynitrite treatment, the autophosphorylation reaction of LCK was performed, and the amount of phosphorylated LIEDNEYTAR was monitored by MRM. About 60% of Tyr394 autophosphorylation was reduced by pretreatment of LCK with 25 μM peroxynitrite (*SI Appendix*, Fig. S4 *H* and *I*). Taken together, the results nominate LCK as a key target for RNS-induced protein nitration as part of the integrated process of T cell suppression by MDSCs.

RNS Neutralization Sensitizes CRPC to Immunotherapy. There is significant up-regulation of 3-NT in human prostate cancer (6–9), consistent with the abundant tumor-infiltrating MDSCs in clinical prostate cancer (21). To assess 3-NT in CRPC, we performed immunohistochemistry (IHC) of 3-NT for a small set of human primary CRPC samples ($n = 15$) and observed that while adjacent normal-like prostate stained negatively, 40% (6/15) of CPRC cases stained positively (Fig. 4*A*). We determined that both cancer cells (pan-cytokeratin$^+$) and T cells (CD3$^+$) were stained positive for 3-NT using IHC costaining (Fig. 4*A*). Consistent with the human sample results, we also detected that both cancer cells (pan-cytokeratin$^+$, strong in Pten/p53/Smad4 tumors, weak in LLC tumors) and T cells (CD3$^+$) were stained positive for 3-NT using IHC costaining for the two mouse models (*SI Appendix*, Fig. S5*A*). We recently showed that the Pten/p53/Smad4 prostate tumors developed into CRPC after surgical castration and enzalutamide treatment, which was refractory to an ICB treatment composed of anti-CTLA4 and anti-PD1 antibodies (21). To determine whether blocking RNS activity using UA would sensitize CRPC to ICB, we enrolled Pten/p53/Smad4 mice into a preclinical trial in a similar fashion as our previous report (21) and treated the randomized cohorts of CRPC-bearing mice with vehicle + isotype IgG (control), anti-CTLA4 and anti-PD1 antibodies (ICB), UA, or ICB + UA for 1 mo. At the endpoint, we observed significant synergistic efficacy by the ICB + UA treatment while ICB or UA alone produced marginal effect (Fig. 4 *B* and *C*). The tumors treated with UA were verified to show significantly reduced 3-NT signals (Fig. 4*D*), and the tumor-infiltrating T cells from UA-treated mice had moderately increased transcriptional level of IL-2, INF-γ, perforin, and granzyme B (*SI Appendix*, Fig. S5*B*). Significant reduction of 3-NT signals in the Pten/p53/Smad4 tumors was also verified when MDSCs were depleted using anti-Gr-1 antibody (*SI Appendix*, Fig. S5*C*), for which the depletion experiment was performed in our recent study (21). This result reinforces the conclusion that MDSCs can account for a large fraction of RNS-induced protein nitration.

We evaluated the effect of ICB, UA, and ICB + UA on the number of infiltrating CD8$^+$ T cells and Foxp3$^+$ Tregs in the

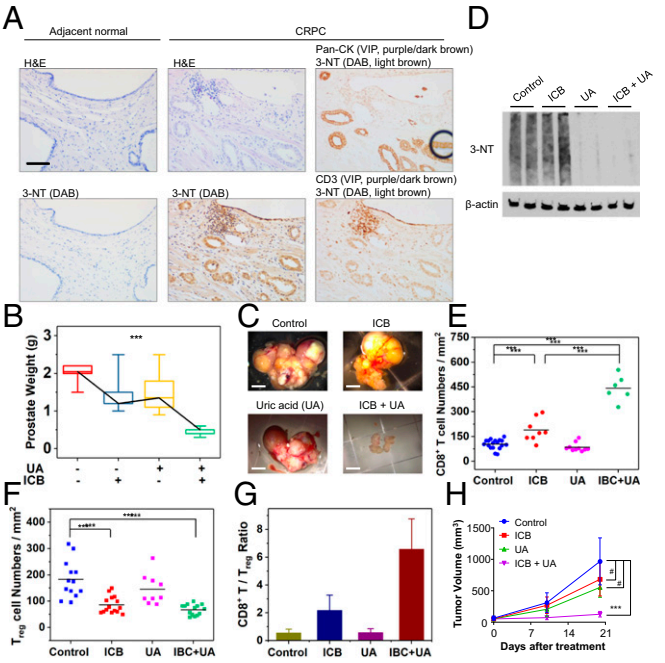

Fig. 4. Combinational therapy of the mouse CRPC and LLC model. (*A*) Representative 3-NT IHC images of adjacent normal or CPRC samples ($n = 15$) and the costaining pattern of 3-NT with pan-cytokeratin (pan-CK) or CD3. (Scale bar, 100 μm.) DAB and VIP refer to 3, 3-diaminobenzidine and violet peroxidase substrate, respectively. The black open circle in top right image was an accidentally trapped air bubble. (*B*) Preclinical trial result of prostate tumor mass of the Pten/p53/Smad4 CRPC model ($n = 6, 5, 6, 5$, respectively). (*C*) Representative prostate images of the preclinical trial in *B*. (Scale bar, 3 mm.) (*D*) Immunoblot analysis of 3-NT levels in whole prostate lysates from the preclinical trial in *B*. (*E*) Quantification of infiltrating CD8$^+$ T cells based on CD8 IHC of CRPC samples from the preclinical trial in *B*. (*F*) Quantification of infiltrating T_{reg} cells based on Foxp3 IHC of CRPC samples from the preclinical trial in *B*. (*G*) Ratios of CD8$^+$ T cell numbers over T_{reg} cell numbers for each treatment condition in the preclinical trial in *B*. (*H*) Preclinical trial result of the LLC s.c. tumor model ($n = 8$–10 for each group). In *B*, ***$P < 0.001$, Mann–Whitney *U* test. In *E*, *F*, and *H*, ***$P < 0.001$, $^{\#}P > 0.05$, Student's *t* test.

treated tumors (*SI Appendix*, Fig. S5*D*) and found that ICB moderately increased CD8$^+$ T cells (Fig. 4*E*) and reduced Foxp3$^+$ Tregs (Fig. 4*F*). Importantly, while UA alone caused no change of infiltration of CD8$^+$ T cells or Tregs, UA elicited strong synergistic effect with ICB to boost the number of infiltrating CD8$^+$ T cells (Fig. 4*E*). As a result, ICB + UA resulted in over sixfold increase of CD8$^+$ T/Treg ratio compared with control, which was threefold increase compared with ICB alone (Fig. 4*G*). UA single treatment did not change the infiltration of myeloid cells or B cells, as shown by IHC of CD11b, Ly6G, F4/80, CD11c, and B220 (*SI Appendix*, Fig. S5*E*). Furthermore, the synergistic antitumor effect by ICB + UA treatment was also observed for the LLC model (Fig. 4*H*). In short, RNS neutralization using UA synergizes with ICB to induce strong antitumor effect in both CRPC and lung cancer models.

Discussion

Here, by applying a nitroproteomic approach to two mouse tumor models, we identified specific nitration of LCK(Tyr394) by intratumoral MDSCs as a mechanism of immunosuppression. Neutralizing RNS was shown as an effective strategy to combine with ICB to elicit strong tumor inhibitory effect in the models, a result with clinical implications in combating emerging resistance to cancer immunotherapy.

The composition of Gr-MDSCs and Mo-MDSCs in the two models differs: while Gr-MDSCs account for over 90% of total MDSCs in the Pten/p53/Smad4 tumors (21), Gr-MDSCs and Mo-MDSCs are comparable in the LLC tumors (*SI Appendix*, Fig. S1*C*). While Mo-MDSCs secreted a higher level of nitrite

(*SI Appendix*, Fig. S1*D*), studies have shown that RNS is essential for Gr-MDSCs to inhibit T cells (4), and the basal NOS activity (primarily by eNOS) is sufficient for Gr-MDSCs to produce RNS (14). Therefore, despite variation of MDSC composition, both models showed strong RNS activity and induced LCK nitration in infiltrating T cells.

Our nitroproteomic method improves on two aspects: first, dimethyl labeling is used for primary amine blocking; second, after reduction, the newly generated amine group on the phenolic ring is conjugated with NHS-S-S-biotin reagent and further labeled with IAA, which can enhance the ionization efficiency of the final product. We used Ang II as a model peptide to study nitration modification. The two characteristic peaks (y_2 ion, immonium ion of His) facilitated identification of intermediate products during the chemical reaction steps, due to their existence independent of Tyr residue changes and N terminus blocking. After dimethyl labeling, the fragmentation pattern became complicated due to c_0 and α cleavage at the N terminus of the peptides (*SI Appendix*, Fig. S2 *D–F*), which was deduced to represent six series of ions (a, b, a-c_0, b-c_0, a-c_0-α, and b-c_0-α) on MS/MS. Similar to other nitroproteomic approaches, our method is limited by its suboptimal sensitivity. Future improvement is needed to allow detection of hundreds of endogenously nitrated proteins.

For LCK, phosphorylation on Tyr394 and Tyr505 plays opposite roles in regulating the kinase activity (24). Our result showed that RNS down-regulates phosphorylation at both sites in T cells, which should predict loss of overall LCK activity. This prediction was verified with the observation of reduced LCK enzymatic activity and autophosphorylation at Tyr394 (Fig. 3*G* and *SI Appendix*, Fig. S4 *H* and *I*). The precise mechanism for nitration-induced impairment of LCK phosphorylation awaits further investigation because it is possible that nitration interferes with phosphorylation through either directly lowering pK_a of the hydroxyl group or indirect conformational change of the protein. An interesting observation of the nitration-activity relationship of LCK was the activity rise at higher peroxynitrite concentration (100–1000 μM), which is likely due to S-nitrosylation of cysteine residues based on studies of another Src family member, HCK (27). At high concentrations (>100 μM), peroxynitrite induces apoptosis in various cell types (11). Therefore, the net effect of peroxynitrite on T cells is inhibition. Because LCK(Tyr394) is a site for both nitration and phosphorylation, it is technically challenging to show that abolishing nitro-Tyr394, but not phospho-Tyr394, impairs T cell activation in vivo.

Given that MDSC targeting is most likely applied in a combinatorial therapeutic setting, we reason that drugs that block MDSC function and display favorable safety profiles would bring the most benefits. Our data indicate that peroxynitrite scavenger is a promising agent to combine with ICB. A previous study also demonstrated that UA enhanced a cancer vaccine therapy in the murine MC38 model (14). These data should prompt clinical studies exploring the benefit of combining RNS-reducing agents with immunotherapy. Last, although MDSCs appear to be a stronger producer of RNS than TAMs in the two models (*SI Appendix*, Fig. S1 *E* and *F*), we do not rule out the possibility that the combination therapy efficacy may be a collective effect of targeting immunosuppressive mechanisms from multiple immune populations including MDSCs as well as M2-polarized TAMs.

Materials and Methods

Animal study was approved and overseen by University of Notre Dame Institutional Animal Care and Use Committee. The *PB-Cre*$^+$ *Pten*$^{L/L}$ *p53*$^{L/L}$ *Smad4*$^{L/L}$ model (Pten/p53/Smad4) with and without the *mTmG* reporter was developed previously (21, 22). Mouse cell line Lewis Lung Carcinoma (LLC) and human cell lines Jurkat and J.CaM1.6 were purchased from American Type Culture Collection (ATCC) and maintained in Dulbecco's Modified Eagle Medium (DMEM) and Roswell Park Memorial Institute (RPMI) 1640 with 10% fetal bovine serum, respectively. Other detailed methods, including chemical reactions of Ang II; LC-MS/MS analysis; MRM assay; clinical samples; isolation of MDSC, macrophages, and T cells; measurements of nitrite concentration, LCK kinase activity, and IL2 production; combination therapy in mice; and statistics are available in *SI Appendix, Supplementary Materials and Methods*.

ACKNOWLEDGMENTS. We thank all members of the Xin Lu laboratory for helpful discussions. This work was supported by American Cancer Society Institutional Research Grant IRG-14-195-01 (M. Sharon Stack is Principal Investigator; Xin Lu is a subrecipient investigator), the Indiana Clinical and Translational Sciences Institute (CTSI), which is funded in part by Grants KL2 TR002530 and UL1 TR002529 (Anantha Shekhar is Principal Investigator; Xin Lu is a recipient of Core Pilot Award) from the National Institutes of Health, National Center for Advancing Translational Sciences, Clinical and Translational Sciences Award. Xin Lu is a recipient of Indiana Clinical and Translational Sciences Institute (CTSI) Early Career Investigator Awards (KL2) Young Investigator Award. S.F. is supported by Walther Cancer Foundation Advancing Basic Cancer grants. X.C. is supported by Ph.D Innovation Fund (BXJ201709) and Visiting Programs for Graduate Students of Shanghai Jiaotong University School of Medicine.

1. Sharma P, Hu-Lieskovan S, Wargo JA, Ribas A (2017) Primary, adaptive, and acquired resistance to cancer immunotherapy. *Cell* 168:707–723.
2. Gabrilovich DI, Nagaraj S (2009) Myeloid-derived suppressor cells as regulators of the immune system. *Nat Rev Immunol* 9:162–174.
3. Gabrilovich DI, Ostrand-Rosenberg S, Bronte V (2012) Coordinated regulation of myeloid cells by tumours. *Nat Rev Immunol* 12:253–268.
4. Raber PL, et al. (2014) Subpopulations of myeloid-derived suppressor cells impair T cell responses through independent nitric oxide-related pathways. *Int J Cancer* 134:2853–2864.
5. De Sanctis F, et al. (2014) The emerging immunological role of post-translational modifications by reactive nitrogen species in cancer microenvironment. *Front Immunol* 5:69.
6. Kasic T, et al. (2011) Modulation of human T-cell functions by reactive nitrogen species. *Eur J Immunol* 41:1843–1849.
7. Molon B, et al. (2011) Chemokine nitration prevents intratumoral infiltration of antigen-specific T cells. *J Exp Med* 208:1949–1962.
8. Bronte V, et al. (2005) Boosting antitumor responses of T lymphocytes infiltrating human prostate cancers. *J Exp Med* 201:1257–1268.
9. Thomas LN, Merrimen J, Bell DG, Rendon R, Too CK (2015) Prolactin- and testosterone-induced carboxypeptidase-D correlates with increased nitrotyrosines and Ki67 in prostate cancer. *Prostate* 75:1726–1736.
10. Radi R (2018) Oxygen radicals, nitric oxide, and peroxynitrite: Redox pathways in molecular medicine. *Proc Natl Acad Sci USA* 115:5839–5848.
11. Szabó C, Ischiropoulos H, Radi R (2007) Peroxynitrite: Biochemistry, pathophysiology and development of therapeutics. *Nat Rev Drug Discov* 6:662–680.
12. Monteiro HP, Arai RJ, Travassos LR (2008) Protein tyrosine phosphorylation and protein tyrosine nitration in redox signaling. *Antioxid Redox Signal* 10:843–889.
13. Monteiro HP (2002) Signal transduction by protein tyrosine nitration: Competition or cooperation with tyrosine phosphorylation-dependent signaling events? *Free Radic Biol Med* 33:765–773.
14. Nagaraj S, et al. (2007) Altered recognition of antigen is a mechanism of CD8+ T cell tolerance in cancer. *Nat Med* 13:828–835.
15. Brito C, et al. (1999) Peroxynitrite inhibits T lymphocyte activation and proliferation by promoting impairment of tyrosine phosphorylation and peroxynitrite-driven apoptotic death. *J Immunol* 162:3356–3366.
16. Batthyány C, et al. (2017) Tyrosine-nitrated proteins: Proteomic and bioanalytical aspects. *Antioxid Redox Signal* 26:313–328.
17. Feeney MB, Schöneich C (2013) Proteomic approaches to analyze protein tyrosine nitration. *Antioxid Redox Signal* 19:1247–1256.
18. Zhan X, Wang X, Desiderio DM (2015) Mass spectrometry analysis of nitrotyrosine-containing proteins. *Mass Spectrom Rev* 34:423–448.
19. Dekker F, Abello N, Wisastra R, Bischoff R (2012) Enrichment and detection of tyrosine-nitrated proteins. *Curr Protoc Protein Sci* Chap 14:Unit 14.13.
20. Beer TM, et al. (2017) Randomized, double-blind, phase III trial of ipilimumab versus placebo in asymptomatic or minimally symptomatic patients with metastatic chemotherapy-naive castration-resistant prostate cancer. *J Clin Oncol* 35:40–47.
21. Lu X, et al. (2017) Effective combinatorial immunotherapy for castration-resistant prostate cancer. *Nature* 543:728–732.
22. Ding Z, et al. (2012) Telomerase reactivation following telomere dysfunction yields murine prostate tumors with bone metastases. *Cell* 148:896–907.
23. Youn JI, Nagaraj S, Collazo M, Gabrilovich DI (2008) Subsets of myeloid-derived suppressor cells in tumor-bearing mice. *J Immunol* 181:5791–5802.
24. Abraham N, Veillette A (1990) Activation of p56lck through mutation of a regulatory carboxy-terminal tyrosine residue requires intact sites of autophosphorylation and myristylation. *Mol Cell Biol* 10:5197–5206.
25. Bartelt RR, Cruz-Orcutt N, Collins M, Houtman JCD (2009) Comparison of T cell receptor-induced proximal signaling and downstream functions in immortalized and primary T cells. *PLoS One* 4:e5430.
26. Straus DB, Weiss A (1992) Genetic evidence for the involvement of the lck tyrosine kinase in signal transduction through the T cell antigen receptor. *Cell* 70:585–593.
27. Mallozzi C, Di Stasi MA, Minetti M (2001) Peroxynitrite-dependent activation of src tyrosine kinases lyn and hck in erythrocytes is under mechanistically different pathways of redox control. *Free Radic Biol Med* 30:1108–1117.